crystals

MDPI

*Article*

# Study of the Bandgap and Crystal Structure of $Cu_4TiSe_4$: Theory vs. Experiment

**Grzegorz Matyszczak [1,*], Szymon Sutuła [2], Paweł Jóźwik [3], Krzysztof Krawczyk [1] and Krzysztof Woźniak [2]**

[1] Department of Chemical Technology, Faculty of Chemistry, Warsaw University of Technology, Noakowskiego Street 3, 00-664 Warsaw, Poland
[2] Faculty of Chemistry, University of Warsaw, Paustera Street 1, 02-097 Warsaw, Poland
[3] Faculty of Advanced Technologies and Chemistry, Military University of Technology, Gen. Sylwestra Kaliskiego Street 2, 00-908 Warsaw, Poland
* Correspondence: grzegorz.matyszczak@pw.edu.pl

**Abstract:** The aim of this study was to investigate the crystal structure and bandgap of the emerging material $Cu_4TiSe_4$ using both theoretical and experimental methods. We synthesized the title compound via solid-state synthesis from elements. The occurrence of the single crystals of the $Cu_4TiSe_4$ compound was proven by X-ray diffraction and EDX investigations. The resolved crystal structure proves the one recently reported for this compound. Additionally, we utilized the Uspex evolutionary algorithm for the prediction of the crystal structure of the $Cu_4TiSe_4$ compound and to check for the presence of potential polymorphs. It turns out that $Cu_4TiSe_4$ may theoretically occur in three different crystal structures (space groups: *I-42m* (no. 121), *R3m* (no. 160), and *P-43m* (no. 215)), in which the rhombohedral phase has the lowest energy. The ab initio study of the bandgap of $Cu_4TiSe_4$ showed that it is indirect for each polymorphic structure and varies in the range of 1.23–1.26 eV, while experimental investigation revealed a direct transition of energy of 1.35 eV, thus showing the potential of this compound for solar cell applications. Theoretical calculations suggested that the rhombohedral phase of $Cu_4TiSe_4$ should exhibit a negative or relatively low (0.64 eV) bandgap.

**Keywords:** tetracopper tetraselenotitanate; $Cu_4TiSe_4$; Uspex; density functional theory; solid state synthesis; bandgap

check for updates

**Citation:** Matyszczak, G.; Sutuła, S.; Jóźwik, P.; Krawczyk, K.; Woźniak, K. Study of the Bandgap and Crystal Structure of $Cu_4TiSe_4$: Theory vs. Experiment. *Crystals* **2023**, *13*, 331. https://doi.org/10.3390/cryst13020331

Academic Editors: Danny A Rehn, Ann E. Mattsson, Roxanne Tutchton, Jian-Xin Zhu and Christopher Lane

Received: 17 January 2023
Revised: 9 February 2023
Accepted: 11 February 2023
Published: 16 February 2023

**Copyright:** © 2023 by the authors. Licensee MDPI, Basel, Switzerland. This article is an open access article distributed under the terms and conditions of the Creative Commons Attribution (CC BY) license (https://creativecommons.org/licenses/by/4.0/).

## 1. Introduction

Wide practical applications of materials are the driving force of materials science. Advanced materials may be utilized in many ways, e.g., as electrodes in Li-ion batteries and sensors, as absorbing materials in solar cells, and as catalysts in chemical reactions of industrial value [1–6]. Investigated inorganic materials are diverse in chemical composition, from binary compounds (e.g., SnS and $SnS_2$), through ternary (e.g., $SrTiO_3$ and $Cu_3VSe_4$), quaternary (e.g., $Cu_2ZnSnS_4$), and even more complex compounds [4–6]. More than just experimental methods are used in the research on important materials, computational methods also utilize ab initio calculations and machine learning algorithms and have even created a new discipline named materials informatics—merging materials science with informatics [7,8].

The structural and chemical aspects of materials are also very important. Knowing the structure or chemical composition of one interesting material, it is possible to derive its analog (structural or chemical) with similar or even better properties. For example, kesterite $Cu_2ZnSnS_4$ is characterized by properties good for applications in photovoltaics, but its features may be improved (according to ab initio calculations) by substituting $Sn^{4+}$ cations with $Ti^{4+}$ cations to form the analogous compound $Cu_2ZnTiS_4$ [9,10]. In addition, both compounds contain similar tetrahedral anions, $SnS_4^{4-}$ and $TiS_4^{4-}$, balanced with $Cu^+$ and $Zn^{2+}$ cations.

Tetrahedral anions $TiSe_4^{4-}$, analogous to $TiS_4^{4-}$, were reported for the first time in compound $Tl_4TiSe_4$ and then in compound $Na_4TiSe_4$, both crystallizing in the monoclinic system [11,12]. Changing the cation to $Cu^+$ gives $Cu_4TiSe_4$—a compound with a cubic structure [13]. Recent studies of tetracopper tetraselenotitanate, $Cu_4TiSe_4$, show its utility due to its exhibition of ultralow lattice thermal conductivity, a bandgap value lying in the optimal range for solar absorber material, and a light absorption coefficient in the visible range greater than $10^5$ $cm^{-1}$, making it a promising thermoelectric and solar energy material [13,14].

In the present study, we investigated the crystal structure and bandgap of $Cu_4TiSe_4$ using both theoretical and experimental methods. We obtained single crystals of $Cu_4TiSe_4$ through a solid-state synthesis. The crystal structure of $Cu_4TiSe_4$ was investigated using X-ray diffraction while SEM and EDX techniques were utilized for visualization of the morphology of crystals and corroboration of their elemental composition [15,16]. We also studied $Cu_4TiSe_4$ with theoretical methods, utilizing the Uspex evolutionary algorithm for crystal structure prediction [15,16]. The crystal structures proposed by the Uspex algorithm were then locally optimized with density functional calculations and utilized in calculations of band structure, exploiting two different approximations [15,16]. The bandgap of crystalline $Cu_4TiSe_4$ was additionally experimentally investigated. Finally, we presented three new theoretical polymorphs of $Cu_4TiSe_4$, justified their potential for applications in solar cells, and proved one of the cubic crystal structures of $Cu_4TiSe_4$ (*P-43m*) in contrast to another (*F-43c*) [13,14].

## 2. Materials and Methods

### *2.1. Solid State Synthesis*

The single crystals of $Cu_4TiSe_4$ were produced through the reaction of elements for the synthesis of the $Cu_2TiSe_4$ compound. In total, 45 mg of Cu (powder, 99.7%, Aldrich Chemistry, St. Louis, MO, USA), 17 mg of Ti (powder, 99.98%, Aldrich Chemistry), and 113 mg of Se (powder, pure for analysis, POCh, Warsaw, Poland) were placed in a quartz ampoule of 60 mm length, 5 mm inner diameter, and 1 mm thickness. Iodine (crystals, pure for analysis, POCh), 2 mg, was additionally used as the transporting agent. The ampoule was evacuated (approximate pressure 10 mbar) and flame-sealed.

The process was carried out in a horizontal tube furnace (Carbolite, EZS 1200, Neuhausen, Germany) at 600 °C for 14 days. The rate of temperature rising at the beginning of the process was 1 °C per minute. The cooling down after the reaction was free.

### *2.2. X-ray Diffraction*

A single crystal, with relevant quality, of $Cu_4TiSe_4$ was chosen for the X-ray diffraction (Agilent Technologies, Wroclaw, Poland) investigation conducted at T = 100(2) K. It was placed in the MiTeGen micromount with help of paratone-N oil. Diffraction data were measured using the Agilent Technologies SuperNova Dual Source diffractometer with MoKα radiation (λ = 0.71073 Å). The lattice parameters were calculated by the least-squares fit to the optimized setting angles of the reflections measured using the CrysAlis CCD software [17]. The reduction in data was conducted utilizing the CrysAlis RED program [17].

We applied a Gaussian numerical absorption correction utilizing a multifaceted crystal model applied in the SCALE3 ABSPACK scaling algorithm (CrysAlisPro 1.171.39.20a (Rigaku Oxford Diffraction, 2015), Oxford Diffraction Ltd, Abingdon, Oxfordshire, UK) [17].

We solved the structure utilizing the ShelXT structure solution program with Intrinsic Phasing along with Olex2, and then consecutive least-squares refinements were conducted based on full-matrix least-squares on $F^2$ with the application of the SHELXL program (2018/3, Göttingen, Germany) [18–20].

$Cu_4TiSe_4$ crystallizes in the cubic *P-43m* space group, and the structure is assumed to be composed of $Cu^+$, $Ti^{4+}$, and $Se^{2-}$ ions. The crystallographic data are presented in Table 1.

**Table 1.** Crystal data and structure refinement for the investigated compound.

| **Empirical Formula** | **$Cu_4Se_4Ti$** |
|---|---|
| Formula weight | 617.90 |
| Temperature/K | 296.78(10) |
| Crystal system | cubic |
| Space group | *P-43m* |
| $a$/Å | 5.65180(10) |
| $b$/Å | 5.65180(10) |
| $c$/Å | 5.65180(10) |
| $\alpha$/° | 90 |
| $\beta$/° | 90 |
| $\gamma$/° | 90 |
| Volume/Å$^3$ | 180.535(10) |
| Z | 1 |
| $\rho_{calc}$ g/cm$^3$ | 5.683 |
| $\mu$/mm$^{-1}$ | 32.692 |
| $F$(000) | 274.0 |
| Crystal size/mm$^3$ | 0.173 × 0.169 × 0.155 |
| Radiation | MoK$\alpha$ ($\lambda$ = 0.71073) |
| 2Θ range for data collection/° | 7.21 to 71.336 |
| Index ranges | $-9 \leq h \leq 9$, $-9 \leq k \leq 9$, $-8 \leq l \leq 9$ |
| Reflections collected | 4803 |
| Independent reflections | 194 [$R_{int}$ = 0.0881, $R_{sigma}$ = 0.0223] |
| Data/restraints/parameters | 194/0/12 |
| Goodness-of-fit on $F^2$ | 1.239 |
| Final $R$ indexes [$I \geq 2\sigma$ ($I$)] | $R_1$ = 0.0224, $wR_2$ = 0.0576 |
| Final $R$ indexes [all data] | $R_1$ = 0.0241, $wR_2$ = 0.0596 |
| Largest diff. peak/hole/e Å$^{-3}$ | 2.18/−0.49 |
| Flack parameter | 0.01(5) |

The Wyckoff positions, atomic coordinates, and atomic displacement parameters are collected in Table S1 in the Supplemental Material. The values of bond lengths and valence angles are given in Tables S2 and S3 in the Supplemental Material.

We utilized an RTG HZG-4 diffractometer for X-ray powder diffraction experiments. The powder diffraction pattern was recorded by applying a step size of 0.04° and a counting time of 3 s using Cu K-α radiation.

### *2.3. Scanning Electron Microscopy (SEM) and Energy-Dispersive X-ray Spectroscopy (EDX)*

Scanning electron microscopy (Thermo Fisher Scientific, FEI, Hillsboro, OR, USA) investigations were carried out with a Quanta 200 FEI Microscope and Quanta 3D FEG, both equipped with an EDAX unit.

### *2.4. UV-Vis Spectrophotometry*

A part of the synthesized $Cu_4TiSe_4$ crystals was ground exhaustively in an agate mortar and then sonicated (frequency of ultrasound 40 kHz) in ethanol for 10 min to form a stable suspension. The UV-Vis spectrum of the suspension was collected by a UV1600 spectrophotometer (AOE Instruments, Shanghai, China) and then was used to perform analysis based on the Tauc formalism.

### *2.5. Ab Initio and Uspex Calculations*

For the purpose of crystal structure prediction, we utilized the Uspex algorithm (v.10.3, Moscow, Russia) [21,22]. It needs a program performing ab initio computations so the Vienna Ab Initio Simulation Package VASP.5.4.4 was applied [23]. The input for the Uspex

algorithm consists of a file defining the values of parameters crucial for the operation of that algorithm. In each simulation, the following values of parameters were utilized:

1. Optimized thermodynamic potential: enthalpy;
2. Population size: 30;
3. Size of initial population: 40;
4. Maximal number of generations: 40;
5. Portion of structures created by heredity: 0.5;
6. Portion of structures created randomly: 0.2;
7. Portion of structures created by atom mutations: 0.2;
8. Portion of structures created by lattice mutations: 0.1;
9. Number of relaxation steps: 5;
10. Resolutions of the k-points grid for consecutive relaxations steps: 0.12, 0.11, 0.10, 0.09, and 0.08.

An exhaustive explanation of each parameter and the principles of operation of the Uspex algorithm are available in the online Uspex manual [24]. Here, we resume the main principles of its action. In the Uspex algorithm, structures are represented by the fractional coordinates of atoms and by lattice parameters [25]. In each generation, parent structures are chosen. They are the individuals that are the best in terms of a certain thermodynamic potential which is determined by ab initio calculations [25].

In a given generation, the worst structures are rejected, and parent structures are drawn from the remaining individuals [25]. The probability of drawing a certain structure is higher the better the structure is [25]. New structures (individuals) are created from the parents with the application of one of three following operations [25]:

(I) Heredity—it merges two geometrically similar parent structures (in reference to fractional coordinates) while the lattice parameters are the weighted average of the parents;
(II) Permutation—it changes the kind of atom between two randomly picked atoms in the structure;
(III) Mutation—it deforms the elemental cell shape using a random symmetric strain matrix.

The heredity operation allows for wide searches while conserving previously found good fragments of structures [25], permutations help find the optimal ordering of atoms [25], and mutations allow for the better verification of structures similar to parent structures, prevent too early convergence, and incorporate elements of metadynamics [25]. Then, the structures undergo relaxations but before that, they are additionally checked in terms of constraints: all interatomic distances must be greater than a certain minimal value, the measures of angles in the elemental cell have to be between 60° and 120°, and all dimensions of the elemental cell have to be greater than a certain value (e.g., the radius of the biggest atom) [25]. Relaxation (i.e., local optimization) is carried out by external programs (such as Quantum Espresso, VASP, and SIESTA) [25]. Locally optimized structures are preserved and used during the construction of the next generation to which one (or more) of the best structures from the previous generation is passed [25].

For the purpose of increasing the efficiency of computations, we used PAW type (projector augmented wave method) pseudopotentials along with the GGA-PBE (Perdew–Burke–Ernzerhof) approximation for the relaxations (local optimizations) of structures during the operation of the Uspex algorithm [26–28]. These approximations were also applied for calculations of the band structure, as well as the HSE06 approximation which typically gives results in line with the experimental data.

In the pseudopotential method, the core electrons are described by the effective potential acting on the valence electrons [29]. Such an approach leads to the achievement of an accuracy similar to that of the all-electron approach and for that reason, the pseudopotential method is the most used tool for many-electron systems [30]. This is why we have chosen the pseudopotential method over other methods such as PWE, FEM, and FDTD [31].

## 3. Results and Discussion

The powder pattern of the synthesis product confirms that we obtained a new powder pattern phase, unknown in the database, along with some amount of titanium(IV) selenide, $TiSe_2$ (Figure 1; the pattern was simulated using Mercury software [32]). The powder pattern simulated based on the crystal structure of $Cu_4TiSe_4$ resolved in this study fits perfectly to unidentified reflexes, which proves the occurrence of $Cu_4TiSe_4$ in the sample and justifies the resolved structure, described later in the text.

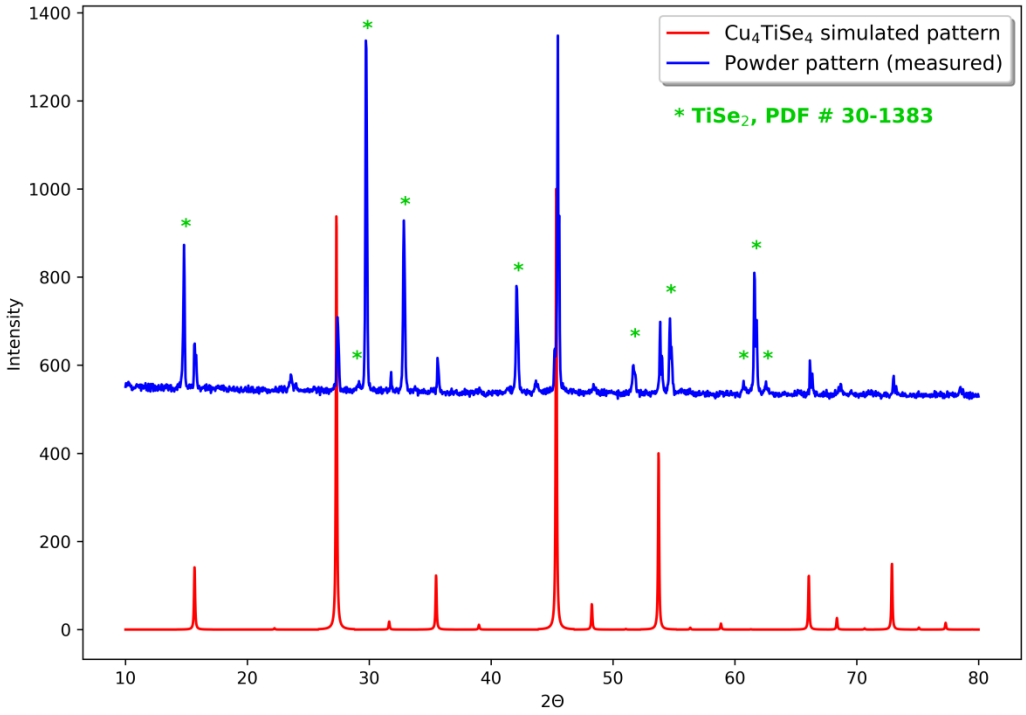



**Figure 1.** Powder diffraction pattern of the product of the conducted synthesis and powder pattern simulated using the resolved crystal structure presented in this study.

The obtained product of synthesis consisted of two distinct phases: a black one and a glossy brown one. Portions of these two phases were observed under scanning electron microscopy. SEM images of both samples, recorded using backscattered electrons, revealed their compositional homogeneity (Figure 2A,B). The outcome of the energy-dispersive X-ray spectroscopy investigation of crystals, shown in Figure 2, proves that the black phase (Figure 2A) is composed of Cu, Ti, and Se in a ratio of 4:1:4 (the exact ratio of Cu:Ti:Se is 4.3:1:4.2), while the glossy brown phase (Figure 2B) is composed of Ti and Se in a 1:2 ratio (the exact ratio of Ti:Se is 1:1.99). Corresponding EDX spectra and data are provided in the Supplemental Materials.

The X-ray diffraction studies of the single crystals of $Cu_4TiSe_4$ reveal that there are five atom sites in the asymmetric part of the structure—three non-disordered and fully occupied by Ti, Se, and Cu, and two partially occupied by Cu. Occupancy factors for disordered Cu positions were kept free at first (which yielded a $Cu_{4.01}TiSe_4$ composition) and then were constrained so that the overall structure would have a $Cu_4TiSe_4$ composition. Atomic displacement parameters, atomic coordinates, and Wyckoff positions are collected in Table S1 in the Supplemental Material.

The crystal structure of $Cu_4TiSe_4$ may be represented with a cubic grid of $TiSe_4$ tetrahedra that are vertically and horizontally connected with each other through Cu atoms. In the diagonal positions between $TiSe_4$ tetrahedra, space is filled, on average, with one Cu atom that is disordered between a cluster composed of one Cu3 and four Cu2 positions. The arrangement of the atom sites within the unit cell and crystal structure

packing of $Cu_4TiSe_4$ are shown in Figures 3 and 4. Both figures were created utilizing the Mercury program [32].

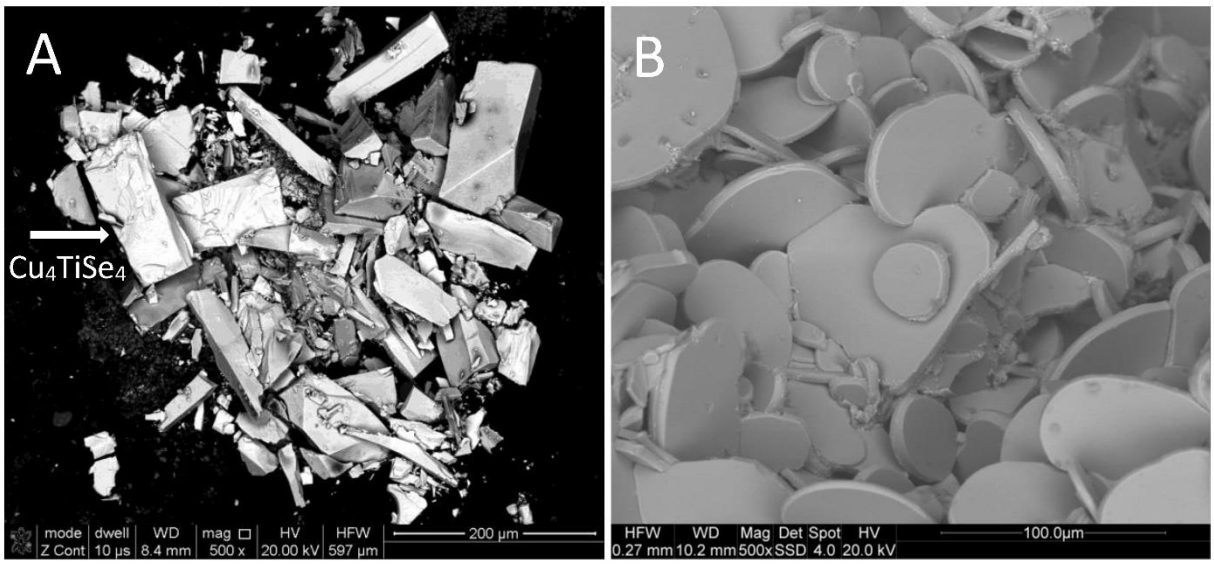



**Figure 2.** Scanning electron microscope images recorded using the backscattered electrons of products of synthesis: (**A**)—black phase ($Cu_4TiSe_4$) and (**B**)—glossy brown phase ($TiSe_2$).

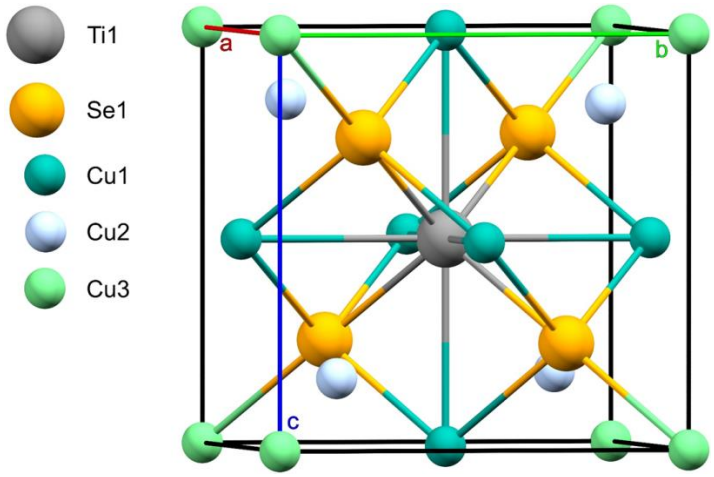



**Figure 3.** Atom sites at the unit cell of $Cu_4TiSe_4$.

The Ti-Se bond lengths are equal to 2.431(1) Å, Ti-Cu equal to 2.826 Å, and Se-Cu are in the range between 2.442 and 2.475(3) Å. The Cu-Cu distances between the Cu1 and Cu2 sites are equal to 2.801(5) Å. Two Cu2 sites are 2.736(14) Å apart, which might allow for the appearance of two Cu atoms within one cluster of disordered Cu and result in induced lattice strain. The values of the valence angles and bond lengths are summarized in Tables S2 and S3 in the Supplemental Material.

The $Cu_4TiSe_4$ crystal structure was first solved by Chen et al. in a cubic *F-43c* space group with a cell parameter $a$ = 11.2936(2) Å [13]. In 2021, Koley et al. corrected the structure, proving extensively that it should be described as *P-43m* with half of the cell parameter $a$ value [14]. We agree with Koley's structure solution, and we solved and refined the crystal structure in the same consecutive steps. In the end, however, we additionally constrained the occupancy factors of Cu atoms so that the structure would have integer numbers in the formula.

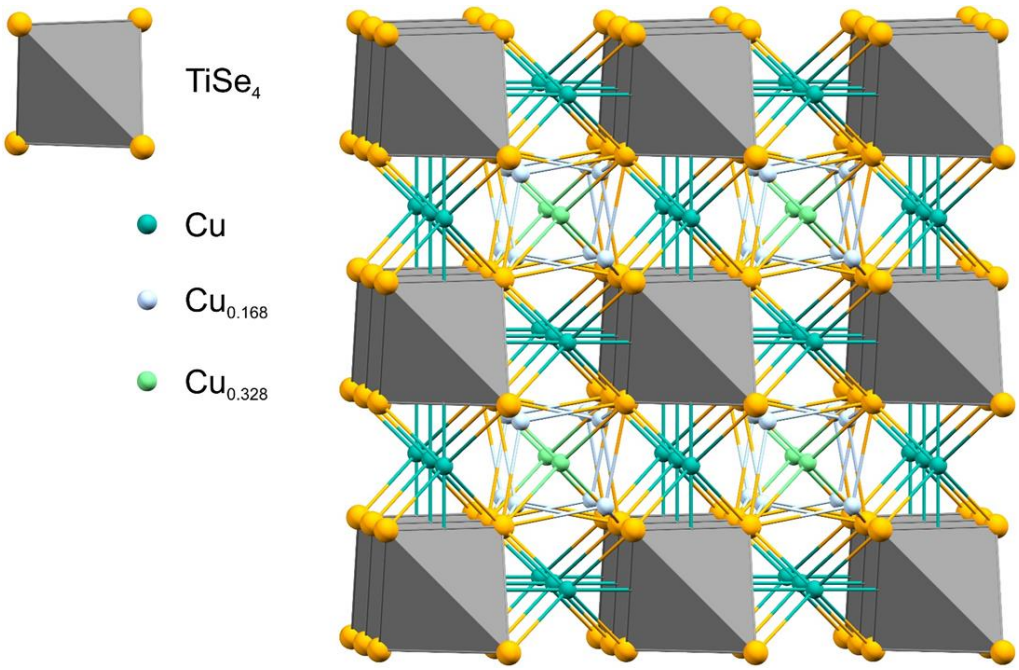



**Figure 4.** Crystal structure of $Cu_4TiSe_4$.

$Cu_4TiSe_4$ is a representative of a copper-metal-chalcogenide (CMC) system that is a class of promising compounds with the potential for application in the field of photovoltaics. From the same family, $Cu_4TiS_4$ has been already described by Klepp et al., and $Cu_2TiTe_3$, $Cu_2ZrTe_3$, and $Cu_2HfTe_3$ have been studied by Keane et al. [33,34]. Choudhury et al. have examined the crystal structure of $Cu_4SnS_4$, and Chen et al. have described the crystal structure of $Cu_4GeS_4$ [35,36]. What is more, the whole family of sulvanite minerals with the formula of $Cu_3MS_4$ (M = V, Nb, Ta) has been extensively studied by many researchers [37,38].

The Uspex algorithm was used to predict the crystal structure of $Cu_4TiSe_4$ and to scrutinize the occurrence of polymorphic structures. Recently, in the case of $Cu_3VSe_4$, it predicted the observed experimentally cubic structure as the global minimum of enthalpy for this chemical composition and—at the same time—it proposed two new theoretical polymorphs [16]. Due to its stochastic nature, the Uspex algorithm was run five times and each time it had no problems with convergence—it finished calculations within a dozen generations. Such a result is far below the allowed maximal limit of generations. The algorithm in each case converged to the same global minimum, which is a rhombohedral crystal structure (space group *R3m*) with an enthalpy value of −41.335 eV, in just several generations. However, the Uspex algorithm also found two other minima of enthalpy corresponding to structures from tetragonal and cubic crystal systems—characterized by space groups *I-42m* and *P-43m*, respectively. The enthalpy values of these two structures are quite different, −41.262 (*I-42m*) and −41.199 eV (*P-43m*). Figure 5 shows the simulated powder diffraction patterns of all the different $Cu_4TiSe_4$ structures found by the Uspex algorithm, proving that they are distinct from each other. Patterns were simulated using Mercury software [32]. The typical experimentally observed crystal structure for the $Cu_4TiSe_4$ compound is the cubic structure, however, the predicted theoretically cubic structure is different from the experimental one (as one may see by comparing the simulated powder patterns in Figures 1 and 5), although it exhibits the same symmetry and very similar lattice parameter (theoretical $a$ = 5.672 Å vs. experimental $a$ = 5.652 Å). The theoretical cubic structure shows no structural disorder.

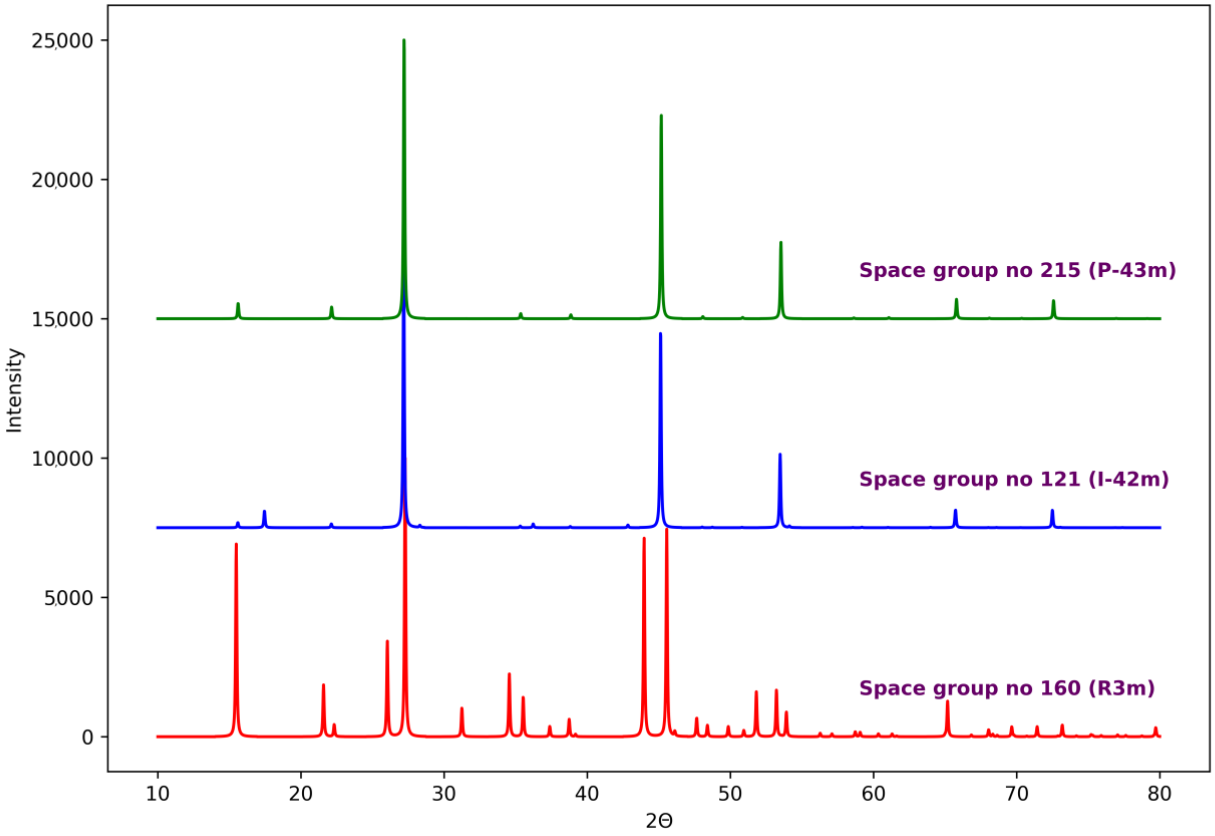



**Figure 5.** Simulated powder diffraction patterns of $Cu_4TiSe_4$ crystal structures calculated by the Uspex algorithm.

The views of four distinct structures (three theoretical and one experimental) along the c-axis reveal intriguing differences among them (Figure 6). It turns out that tetragonal and cubic crystal structures predicted by the Uspex algorithm are quite similar and the difference between them is in the distribution of $Cu^+$ cations—in the cubic structure one can observe strips containing only $Cu^+$ cations while in the tetragonal phase, there are only mixed strips composed of both $Cu^+$ and $Ti^{4+}$ cations. This contributes to the difference in enthalpies between these two structures which is 0.063 eV. Moreover, the rhombohedral structure exhibits a honeycomb pattern which is different from the cubic pattern seen in structures with space groups *I-42m* and *P-43m*. Figure 6 also clearly shows that the difference between the theoretical and experimental cubic structures is the structural disorder occurring in the latter one.

It should be emphasized that the global minimum of enthalpy for the composition $Cu_4TiSe_4$ found by the Uspex algorithm (space group *R3m*) is totally different than the experimentally observed crystal structure (disordered, space group *P-43m*), as revealed in Figure 6. More comparisons of views of crystal structures of $Cu_4TiSe_4$, along the b-axis and reciprocal b-axis, are presented in Figures S3 and S4 in the Supplemental Material. First of all, in the case of the $CdBi_2S_4$ compound, it was shown previously that "the Uspex algorithm is not capable of predicting crystal structures with the structural disorder" [15]. Secondly, the algorithm reached a crystal structure similar to the experimental one in the case of symmetry and lattice parameters, but without the structural disorder (which is characteristic of Uspex) and only as a local minimum of enthalpy. It seems that the rhombohedral theoretical structure is not the real global minimum of enthalpy and thus was not obtained in the synthesis performed in this study. At the same time, the incorporation of structural disorder into the theoretical (ordered) cubic structure likely decreases its enthalpy, making the disordered cubic structure the real global minimum of enthalpy. Interestingly, a phase transition from a disordered cubic *P-43m* structure to a partially

ordered rhombohedral *R3m* structure at −92°C was reported, adding further proof of the usefulness and verifiability of the Uspex algorithm [39].

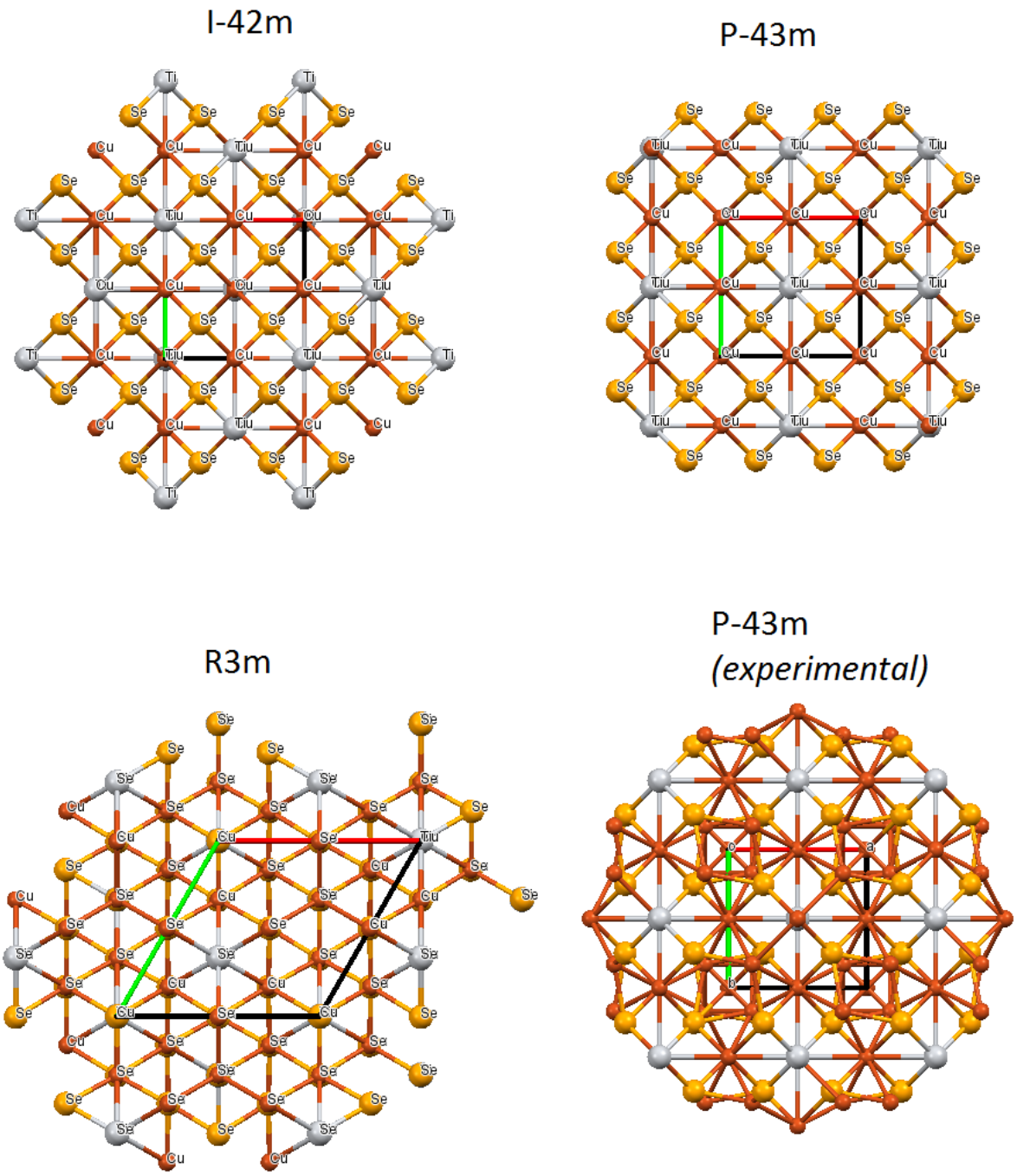



**Figure 6.** A collection of views along the c-axis of $Cu_4TiSe_4$ structures predicted (using the Uspex algorithm) and the experimental structure of $Cu_4TiSe_4$.

The new tetragonal (theoretical) structure of $Cu_4TiSe_4$ is similar to one of the structures accepted by kesterite $Cu_2ZnSnS_4$ [9,10,40,41]. It is, moreover, related to the stannite structure, as they both exhibit the same space group (*I-42m*) and similar relation between the $\boldsymbol{a}$ and $\boldsymbol{c}$ lattice parameters (for stannites $\boldsymbol{c}$:$\boldsymbol{a} \approx 2$) [9,10]. Interestingly, at the same time, the Uspex algorithm for $Cu_4TiSe_4$ does not suggest more structures related to those adopted by kesterites. Table 2 summarizes the data on the $Cu_4TiSe_4$ crystal structures calculated by the Uspex algorithm.

**Table 2.** Summary of data on the $Cu_4TiSe_4$ crystal structures calculated using the Uspex algorithm.

| Space Group Number (Symbol) | Lattice Parameters {Å} | Structure Type | Enthalpy {eV} |
|---|---|---|---|
| 121 (*I-42m*) | $a$ = 5.677, $c$ = 11.358 | Stannite | −41.262 |
| 215 (*P-43m*) | $a$ = 5.672 | - | −41.199 |
| 160 (*R3m*) | $a$ = 7.958, $c$ = 10.258 | - | −41.335 |

The simulated electronic band structures across the high symmetry points of the corresponding Brillouin zones for each theoretical $Cu_4TiSe_4$ polymorph are presented in Figure 7. We compare both approaches—the GGA-PBE and HSE06 approximations.

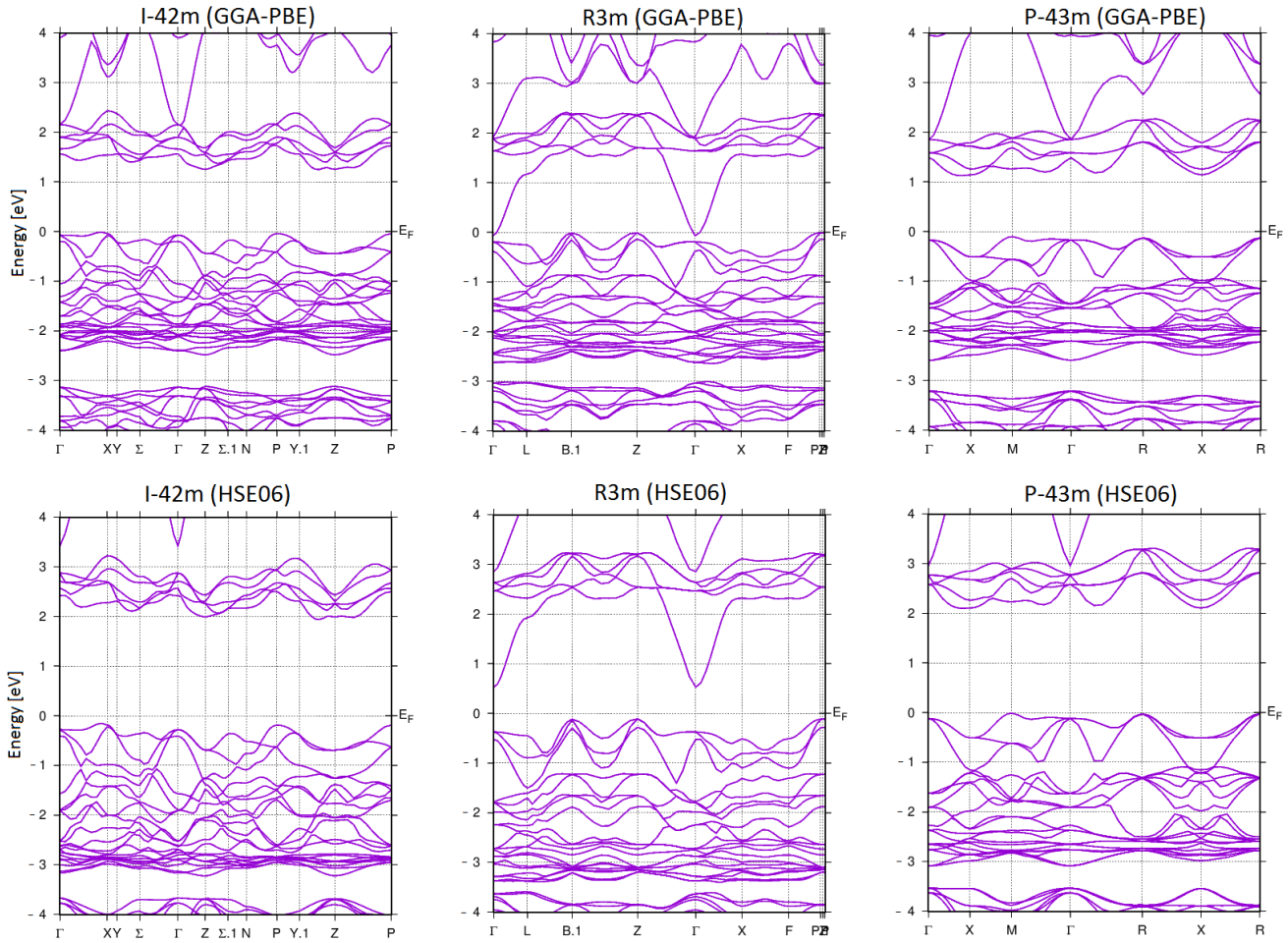



**Figure 7.** Electronic band structures for each $Cu_4TiSe_4$ polymorphic structure simulated using GGA-PBE and HSE06 approaches.

Each polymorphic structure of $Cu_4TiSe_4$ is characterized by a very similar overall profile of the conduction and valence bands in both utilized approximations. Simulated electronic band structures show the existence of band gaps in most cases. The bandgap values computed with the GGA-PBE approximation are 1.26 eV (*I-42m*), 1.23 eV (*P-43m*), and −0.06 eV (*R3m*). At the same time, the values computed with the HSE06 approximation are 2.09 eV (*I-42m*), 2.11 eV (*P-43m*), and 0.64 eV (*R3m*). All band gaps are indirect in type. The GGA-PBE approach underrates the band gap values while the HSE06 approach gives results that are more valid in the case of complex chalcogenide materials, such as kesterites [40]. The values predicted here in the GGA-PBE approximation are closely related to those reported previously for $Cu_4TiSe_4$ in the case of a not-disordered crystal

structure [13,14]. The computational results obtained previously using the GGA-PBE approximation and many-body perturbation theory was in very good agreement with experimental data in term of the indirect bandgap value [13,14]. Therefore, in the case of $Cu_4TiSe_4$, the GGA-PBE approximation is reliable for treating the electronic exchange and correlation, especially when taking into account the accordance between the experimental and theoretical lattice parameters of the cubic structure. However, it is interesting that this approximation simultaneously suggests that $Cu_4TiSe_4$ in the rhombohedral form (the theoretical global minimum of enthalpy) should exhibit metallic behavior due to a negative bandgap; even the HSE06 approximation gives a relatively small value of energy bandgap (0.64 eV) in the case of this polymorph. The tetragonal and cubic polymorphic $Cu_4TiSe_4$ structures are characterized theoretically by bandgap values in the range 1.23–1.26 eV, lying in the optimal range of the Schockley–Queisser limit, which indicates their possible applications in photovoltaics [42]. The bandstructure of disordered cubic $Cu_4TiSe_4$ was calculated previously by both Chen et al. and Koley et al., showing an indirect bandgap value of ca. 1.2 eV, which is very similar to the ordered cubic $Cu_4TiSe_4$ calculated in this study [13,14]. It seems that structural disorder does not affect the value of bandgap very much.

The experimental investigation of the optical bandgap of bulk $Cu_4TiSe_4$ (Figure 8) reveals the direct transition with a bandgap value of 1.35 eV. Such a result is in great correspondence with the value reported before (1.34 eV) by Chen and coauthors and also lies in the optimal range of the Schockley–Queisser limit [13,42]. The indirect transition was not observed in our study.

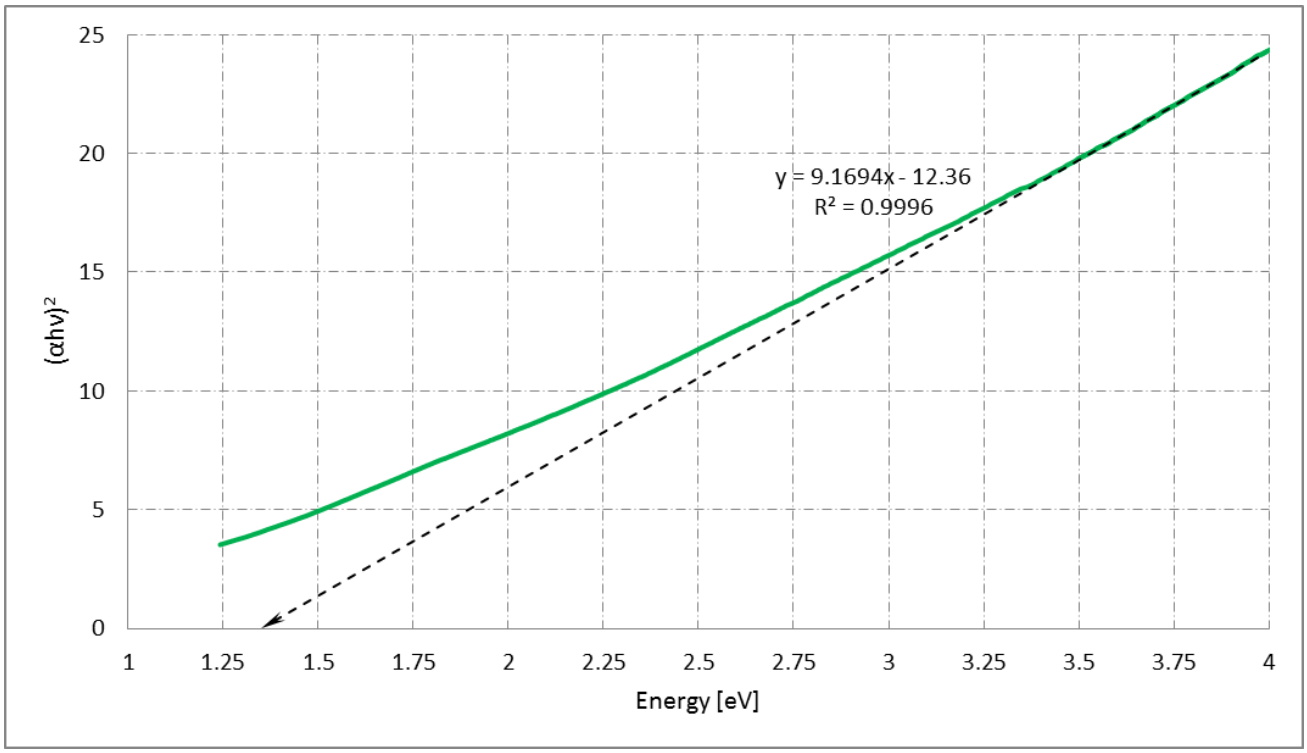



**Figure 8.** The plot of $(\alpha h\nu)^2$ vs. $h\nu$ for a suspension of $Cu_4TiSe_4$ in ethanol.

## 4. Conclusions

We obtained crystals of tetracopper tetraselenotitanate, $Cu_4TiSe_4$, utilizing solid-state synthesis. The elemental composition and crystal structure of the as wis proven by the SEM, EDX, and XRD investigations. The crystal structure of $Cu_4TiSe_4$ shown in this study was characterized by better resolution in comparison with that presented before. A genetic algorithm, Uspex, suggested that $Cu_4TiSe_4$ theoretically may adopt not only a cubic structure but also two other structures—one from the tetragonal system (*I-42m*,

stannite structure) and the second from the rhombohedral system (*R3m*, the theoretical global minimum of enthalpy). However, these structures were not observed experimentally thus far. In the ab initio investigations of $Cu_4TiSe_4$, the GGA-PBE approximation led to lattice parameter values and an indirect energy bandgap very close to the experimental. Studies of the bandgap of $Cu_4TiSe_4$ revealed its potential as a solar energy material—the experimental direct bandgap is 1.35 eV. Such a value is placed in the most optimal range of the Schockley–Queisser limit.

**Supplementary Materials:** The following supporting information can be downloaded at: https://www.mdpi.com/article/10.3390/cryst13020331/s1, Figure S1: The EDX spectrum for $Cu_4TiSe_4$ phase corresponding to Figure 2A in the manuscript.; Figure S2: The EDX spectrum for $TiSe_2$ phase corresponding to Figure 2B in the manuscript.; Figure S3: Collection of views along the b-axis of three structures predicted by the Uspex algorithm and the experimental (disordered) structure of $Cu_4TiSe_4$. (Ti—silver, Cu—brown, Se—yellow); Figure S4: Collection of views along the reciprocal b-axis of three structures predicted by the Uspex algorithm and the experimental (disordered) structure of $Cu_4TiSe_4$. (Ti—silver, Cu—brown, Se—yellow); Table S1: Fractal atomic coordinates and displacement parameters [$Å^2$].; Table S2: Bond lengths for investigated compound.; Table S3: Valence angles for investigated compound.; Table S4: The EDX data for $Cu_4TiSe_4$ phase corresponding to Figure 2A in the manuscript.; Table S5: The EDX data for $TiSe_2$ phase corresponding to Figure 2B in the manuscript.

**Author Contributions:** G.M.: Conceptualization, Methodology, Supervision, Writing—Original draft preparation, Investigation, Writing—Reviewing and Editing, Visualization, Formal analysis. S.S.: Investigation, Writing—Reviewing and Editing, Visualization, Formal analysis. P.J.: Investigation, Visualization, Formal analysis. K.K.: Supervision, Conceptualization. K.W.: Writing-Reviewing and Editing. All authors have read and agreed to the published version of the manuscript.

**Funding:** This scientific research was financed from the budgetary funds on science projected for 2018−2022 as a research project under the "Diamond Grant" program (DI 2017 000847 (ID 397239)). This research was supported in part by PLGrid Infrastructure.

**Institutional Review Board Statement:** Not applicable.

**Informed Consent Statement:** Not applicable.

**Data Availability Statement:** The data are available on request.

**Conflicts of Interest:** The authors declare no conflict of interest.

## References

1. Burton, L.A.; Colombara, D.; Abellon, R.D.; Grozema, F.C.; Peter, L.M.; Savenije, T.J.; Dennler, G.; Walsh, A. Synthesis, Characterization, and Electronic Structure of Single-Crystal SnS, $Sn_2S_3$, and $SnS_2$. *Chem. Mater.* **2013**, *25*, 4908–4916. [CrossRef]
2. Lewis, D.J.; Kevin, P.; Bakr, O.; Muryn, C.A.; Malik, M.A.; O'Brien, P. Routes to tin chalcogenide materials as thin films or nanoparticles: A potentially important class of semiconductor for sustainable solar energy conversion. *Inorg. Chem. Front.* **2014**, *1*, 577–598. [CrossRef]
3. Reddy, N.K.; Devika, M.; Gopal, E.S.R. Review on Tin (II) Sulfide (SnS) Material: Synthesis, Properties, and Applications. *Crit. Rev. Solid State* **2015**, *40*, 359–398. [CrossRef]
4. Zhang, Q.; Ma, S.; Zhang, R.; Tie, Y.; Pei, S. Optimization ethanol detection performance manifested by $SnS/SnS_2$ nanoparticles. *Mater. Lett.* **2019**, *258*, 126783. [CrossRef]
5. Wu, Y.-Q.; Yang, Y.; Pu, H.; Gao, R.-Z.; Meng, W.-J.; Yang, H.-X.; Zhao, D.-L. $SnS_2$ nanoparticle-integrated graphene nanosheets as high-performance and cycle-stable anodes for lithium and sodium storage. *J. Alloy Compd.* **2020**, *822*, 153686. [CrossRef]
6. Tian, H.; Fan, C.; Liu, G.; Yuan, S.; Zhang, Y.; Wang, M.; Li, E. Ultrafast broadband photodetector based on SnS synthesized by hydrothermal method. *Appl. Surf. Sci.* **2019**, *487*, 1043–1048. [CrossRef]
7. Butler, K.T.; Davies, D.W.; Cartwright, H.; Isayev, O.; Walsh, A. Machine learning for molecular and materials science. *Nature* **2018**, *559*, 547–555. [CrossRef]
8. Schleder, G.R.; Padilha, A.C.M.; Acosta, C.M.; Costa, M.; Fazzio, A. From DFT to machine learning: Recent approaches to materials science—A review. *J. Phys. Mater.* **2019**, *2*, 032001. [CrossRef]
9. Song, X.; Ji, X.; Li, M.; Lin, W.; Luo, X.; Zhang, H. A Review on Development Prospect of CZTS Based Thin Film Solar Cells. *Int. J. Photoenergy* **2014**, *2014*, 613173. [CrossRef]

10. Wang, X.; Li, J.; Zhao, Z.; Huang, S.; Xie, W. Crystal structure and electronic structure of quaternary semiconductors $Cu_2ZnTiSe_4$ and $Cu_2ZnTiS_4$ for solar cell absorber. *J. Appl. Phys.* **2012**, *112*, 023701. [CrossRef]
11. Klepp, K.O.; Eulenberger, G. Preparation and Crystal Structure of $Tl_4TiS_4$, $Tl_4SnS_4$, and $Tl_4TiSe_4$. *Z. Naturforsch. B* **1984**, *39*, 705–712. [CrossRef]
12. Klepp, K.O. Preparation and Crystal Structure of $Na_4TiSe_4$. A Selenotitanate with Discrete Tetrahedral Anions. *Z. Naturforsch. B* **2000**, *55*, 39–44. [CrossRef]
13. Chen, E.M.; Williams, L.; Olvera, A.; Zhang, C.; Zhang, M.; Shi, G.; Heron, J.T.; Qi, L.; Guo, L.J.; Kioupakis, E.; et al. Sustainable p-type copper selenide solar material with ultra-large absorption coefficient. *Chem. Sci.* **2018**, *9*, 5405–54144. [CrossRef] [PubMed]
14. Koley, B.; Lakshan, A.; Raghuvanshi, P.R.; Singh, C.; Bhattacharya, A.; Jana, P.P. Ultralow Lattice Thermal Conductivity at Room Temperature in $Cu_4TiSe_4$. *Angew. Chem. Int. Ed.* **2020**, *60*, 9106–9113. [CrossRef]
15. Matyszczak, G.; Sutuła, S.; Krawczyk, K.; Woźniak, K. Experimental and theoretical study of crystal structure and bandgap of CdBi2S4. *J. Solid State Chem.* **2021**, *305*, 122695. [CrossRef]
16. Matyszczak, G.; Sutuła, S.; Januszewski, R.; Zakrzewska, A.; Cieślukowska, K.; Gołędowska, M.; Jóźwik, P.; Woźniak, K. Synthesis, characterization, crystal structure prediction, and ab initio study of bandgap of Cu3VSe4. *J. Solid State Chem.* **2021**, *301*, 122336. [CrossRef]
17. *CrysAlis CCD and CrysAlis RED*; Oxford Diffraction Ltd.: Yarnton, UK, 2008.
18. Dolomanov, O.V.; Bourhis, L.J.; Gildea, R.J.; Howard, J.A.K.; Puschmann, H. OLEX2: A complete structure solution, refinement and analysis program. *J. Appl. Cryst.* **2009**, *42*, 339–341. [CrossRef]
19. Sheldrick, G.M. *SHELXT*—Integrated space-group and crystal-structure determination. *Acta Cryst. A* **2015**, *71*, 3–8 . [CrossRef]
20. Sheldrick, G.M. Crystal structure refinement with *SHELXL*. *Acta Cryst. C* **2015**, *71*, 3–8 . [CrossRef]
21. Zhang, W.; Oganov, A.R.; Goncharov, A.F.; Zhu, Q.; Boulfelfel, S.E.; Lyakhov, A.O.; Stavrou, E.; Somayazulu, M.; Prakapenka, V.B.; Konôpková, Z. Unexpected Stable Stoichiometries of Sodium Chlorides. *Science* **2013**, *342*, 1502–1505. [CrossRef]
22. Zurek, E.; Hoffmann, R.; Ashcroft, N.W.; Oganov, A.R.; Lyakhov, A.O. A little bit of lithium does a lot for hydrogen. *Proc. Natl. Acad. Sci. USA* **2009**, *106*, 17640–17643. [CrossRef]
23. Kresse, G.; Furthmüller, J. Efficient iterative schemes forab initiototal-energy calculations using a plane-wave basis set. *Phys. Rev. B* **1996**, *54*, 11169–11186. [CrossRef] [PubMed]
24. Available online: https://uspex-team.org/en/uspex/documentation (accessed on 8 February 2023).
25. Organov, A.R.; Ma, Y.; Glass, C.W.; Valle, M. Evolutionary crystal structure prediction: Overview of the USPEX method and some of its applications. *PSI-K Newsl.* **2007**, *84*, 142–171.
26. Perdew, J.P.; Burke, K.; Ernzerhof, M. Generalized gradient approximation made simple. *Phys. Rev. Lett.* **1996**, *77*, 3865–3868. [CrossRef] [PubMed]
27. Blöchl, P.E. Projector augmented-wave method. *Phys. Rev. B* **1994**, *50*, 17953–17979. [CrossRef] [PubMed]
28. Kresse, G.; Joubert, D. From ultrasoft pseudopotentials to the projector augmented-wave method. *Phys. Rev. B* **1999**, *59*, 1758–1775. [CrossRef]
29. Phillips, J.C.; Kleinman, L. New Method for Calculating Wave Functions in Crystals and Molecules. *Phys. Rev.* **1959**, *116*, 287–294. [CrossRef]
30. Lejaeghere, K.; Bihlmayer, G.; Björkman, T.; Blaha, P.; Blügel, S.; Blum, V.; Caliste, D.; Castelli, I.E.; Clark, S.J.; Corso, A.D.; et al. Reproducibility in density functional theory calculations of solids. *Science* **2016**, *351*, aad3000. [CrossRef]
31. Chau, Y.-F.; Wu, F.-L.; Jiang, Z.-H.; Li, H.-Y. Evolution of the complete photonic bandgap of two-dimensional photonic crystal. *Opt. Express* **2011**, *19*, 4862–4867. [CrossRef]
32. Macrae, C.F.; Edgington, P.R.; McCabe, P.; Pidcock, E.; Shields, G.P.; Taylor, R.; Towler, M.; van de Streek, J. Mercury: Visualization and analysis of crystal structures. *J. Appl. Crystallogr.* **2006**, *39*, 453–457. [CrossRef]
33. Klepp, K.; Gurtner, D. Synthesis and crystal structure of Cu4TiS4: A novel chalcogenide with tetrahedrally coordinated titanium. *J. Alloy Compd.* **1996**, *243*, 19–22. [CrossRef]
34. Keane, P.M.; Ibers, J.A. Synthesis, structure, and physical properties of the new group IV ternary tellurides, $Cu_2MTe_3$ (M = Ti, Zr, Hf). *J. Solid State Chem.* **1991**, *93*, 291–297. [CrossRef]
35. Choudhury, A.; Mohapatra, S.; Asl, H.Y.; Lee, S.H.; Hor, Y.S.; Medvedeva, J.E.; McClane, D.L.; Hilmas, G.E.; McGuire, M.A.; May, A.F.; et al. New insights into the structure, chemistry, and properties of $Cu_4SnS_4$. *J. Solid State Chem.* **2017**, *253*, 192–201. [CrossRef]
36. Anchena, X.; Onodaa, M.; Wada, H.; Satoa, A.; Nozakia, H.; Irmerb, R.H. Preparation, Electrical Properties, Crystal Structure, and Electronic Structure of $Cu_4GeS_4$. *J. Solid State Chem.* **1999**, *145*, 204–211. [CrossRef]
37. van Arkel, A.E.; Crevecoeur, C. Quelques sulfures et seleniures complexes. *J. Less Common Met.* **1963**, *5*, 177–180. [CrossRef]
38. Klepp, O.; Gurtner, D. Crystal structure of tricopper tetraselenidovanadate(V), $Cu_3VSe_4$. *Z. Kristallogr. NCS* **2000**, *215*, 4. [CrossRef]
39. Koley, B.; Lakshan, A.; Jana, P.P. Temperature-Induced Phase Transition in $Cu_4TiSe_4$. *Eur. J. Inorg. Chem.* **2021**, *2021*, 5052–5059. [CrossRef]
40. Matyszczak, G.; Zberecki, K. Application of artificial neural network and global optimization techniques for high throughput modeling of the crystal structure of stannites and kesterites. *J. Comput. Chem.* **2021**, *42*, 740–745. [CrossRef]

41. Chen, S.; Gong, X.G.; Walsh, A.; Wei, S.-H. Crystal and electronic band structure of $Cu_2ZnSnX_4$ (X=S and Se) photovoltaic absorbers: First-principles insights. *Appl. Phys. Lett.* **2009**, *94*, 041903. [CrossRef]
42. Shockley, W.; Queisser, H.J. Detailed Balance Limit of Efficiency of p-n Junction Solar Cells. *J. Appl. Phys.* **1961**, *32*, 510–519. [CrossRef]

**Disclaimer/Publisher's Note:** The statements, opinions and data contained in all publications are solely those of the individual author(s) and contributor(s) and not of MDPI and/or the editor(s). MDPI and/or the editor(s) disclaim responsibility for any injury to people or property resulting from any ideas, methods, instructions or products referred to in the content.